

## Research Article

**Cite this article:** Mangini M *et al.* (2024) Application of Raman spectroscopy to the evaluation of F-actin changes in sea urchin eggs at fertilization. *Zygote*. **32**: 38–48. doi: [10.1017/S0967199423000552](https://doi.org/10.1017/S0967199423000552)

Received: 20 June 2023

Revised: 22 September 2023

Accepted: 29 September 2023

First published online: 5 December 2023

**Keywords:**

Actin; Fertilization; LifeAct-GFP; Raman microspectroscopy; Sea urchin eggs



**Corresponding authors:**

Anna Chiara De Luca;

Email: [annachiara.deluca@cnr.it](mailto:annachiara.deluca@cnr.it);

Luigia Santella; Email: [santella@szn.it](mailto:santella@szn.it)

# Application of Raman spectroscopy to the evaluation of F-actin changes in sea urchin eggs at fertilization

Maria Mangini<sup>1</sup> , Nunzia Limatola<sup>2</sup>, Maria Antonietta Ferrara<sup>3</sup>, Giuseppe Coppola<sup>3</sup>, Jong Tai Chun<sup>4</sup>, Anna Chiara De Luca<sup>1</sup> and Luigia Santella<sup>2</sup> 

<sup>1</sup>Institute of Experimental Endocrinology and Oncology ‘G. Salvatore’, Second Unit, National Research Council, 80131 Naples, Italy; <sup>2</sup>Department of Research Infrastructures for Marine Biological Resources, Stazione Zoologica Anton Dohrn, 80121 Naples, Italy; <sup>3</sup>Institute of Applied Sciences and Intelligent Systems ‘E. Caianiello’, Unit of Naples, National Research Council, 80131 Naples, Italy and <sup>4</sup>Department of Biology and Evolution of Marine Organisms, Stazione Zoologica Anton Dohrn, 80121 Naples, Italy

**Summary**

The actin filaments on the surface of echinoderm oocytes and eggs readily undergo massive reorganization during meiotic maturation and fertilization. In sea urchin eggs, the actin cytoskeletal response to the fertilizing sperm is fast enough to accompany  $\text{Ca}^{2+}$  signals and to guide sperm's entry into the egg. Although recent work using live cell imaging technology confirmed changes in the actin polymerization status in fertilized eggs, as was previously shown using light and electron microscopy, it failed to provide experimental evidence of F-actin depolymerization a few seconds after insemination, which is concurrent with the sperm-induced  $\text{Ca}^{2+}$  release. In the present study, we applied Raman microspectroscopy to tackle this issue by examining the spectral profiles of the egg's subplasmalemmal regions before and after treating the eggs with actin drugs or fertilizing sperm. At both early (15 s) and late (15 min) time points after fertilization, specific peak shifts in the Raman spectra revealed change in the actin structure, and Raman imaging detected the cytoskeletal changes corresponding to the F-actin reorganization visualized with LifeAct-GFP in confocal microscopy. Our observation suggests that the application of Raman spectroscopy, which does not require microinjection of fluorescent probes and exogenous gene expression, may serve as an alternative or even advantageous method in disclosing rapid subtle changes in the subplasmalemmal actin cytoskeleton that are difficult to resolve.

**Introduction**

Since the end of the 19th century, echinoderm gametes have been extensively used as model systems to study oocyte maturation, sperm activation, species-specific sperm–egg interaction, as well as structural, electrical, and  $\text{Ca}^{2+}$  changes regulating signal transduction events at fertilization necessary for normal embryonic development (Kanatani, 1973; Meijer and Guerrier, 1984; Trimmer and Vacquier, 1986; Wessel *et al.*, 2001; Santella *et al.*, 2012; Santella and Chun, 2022). Indeed, due to the availability of large amounts of gametes that can be allowed to undergo external fertilization in seawater, starfish and sea urchins have offered numerous advantages for performing experiments related to sexual reproduction.

In starfish, oocyte maturation can be induced *in vitro* using 1-methyladenine, which is a significant advantage in studying the conditions of fertilizability acquired during meiotic maturation (Chun *et al.*, 2018; Kishimoto, 2018; Chiba, 2020; Santella *et al.*, 2020; Santella and Chun, 2022). Conversely, sea urchins have facilitated studies on fertilization and early embryonic development due to the easiness of handling mature eggs and their synchronous cleavages (Steinhardt *et al.*, 1971; Epel, 1978; Trimmer and Vacquier, 1986; Wessel *et al.*, 2001; Vacquier, 2011). Moreover, echinoderm eggs have a large diameter and transparent cytoplasm, which makes them particularly suitable for imaging experiments that utilize fluorescent molecular probes. In laboratories, to facilitate electrophysiological measurements,  $\text{Ca}^{2+}$  detection, and the visualization of structural changes on the egg surface at fertilization, sea urchin eggs were often deprived of their external layers (jelly and vitelline) or attached to polylysine-coated glasses. Indeed, these ‘dejailed or denuded eggs’ may adhere better to solid substrates and are relatively immobilized during sperm-induced egg activation (Epel *et al.*, 1970; Steinhardt *et al.*, 1971; Mazia *et al.*, 1975; Schatten and Mazia, 1976). However, this manipulation or treatment of the egg surface may inevitably alter the egg's morphology and physiology, leading to a fertilization response that may differ from natural conditions (Just, 1939). In line with this, in recent studies investigating the role of the structural dynamics of the actin cytoskeleton of the egg cortex in the fertilization response, only ‘intact eggs’ of sea urchin

© The Author(s), 2023. Published by Cambridge University Press. This is an Open Access article, distributed under the terms of the Creative Commons Attribution licence (<http://creativecommons.org/licenses/by/4.0/>), which permits unrestricted re-use, distribution and reproduction, provided the original article is properly cited.



CAMBRIDGE  
UNIVERSITY PRESS



have been used for imaging  $\text{Ca}^{2+}$ , F-actin changes, and sperm incorporation into the zygotes in combination with light and electron microscopy (Chun *et al.*, 2014; Limatola *et al.*, 2019, 2020b, 2021b; Vasilev *et al.*, 2019).

In sea urchins, 'egg activation' by the fertilizing sperm includes a rapid influx of  $\text{Ca}^{2+}$  over the entire surface of the egg a few seconds after the fusion of the sperm with the egg plasma membrane (cortical flash, CF) and a subsequent increase of intracellular  $\text{Ca}^{2+}$  level ( $\text{Ca}^{2+}$  wave, CW; Whitaker, 2006; Parrington *et al.*, 2007; Ramos and Wessel, 2013). Recent studies have indicated that the early CF event strictly depends on the actin-based microvillar morphology and microfilaments associated with the cortical granules (CG; Spudich *et al.*, 1988; Chun *et al.*, 2014; Vasilev *et al.*, 2019). The following CW with a precise spatiotemporal pattern of  $\text{Ca}^{2+}$  release is concomitant with the dissolution (or superficial cytolysis) of the egg's cortical region (ectoplasm) and the breakdown of the CG positioned just below the plasma membrane (Just, 1939; Gillot *et al.*, 1991; Santella *et al.*, 2015; Vasilev *et al.*, 2019). The extrusion of the contents of CG promotes the separation of the vitelline layer bound to the plasma membrane covering microvilli, resulting in the lifting of the newly formed fertilization envelope (FE). Then, the  $\text{Ca}^{2+}$  increase induces a dramatic reorganization of the egg cortex, including microvilli elongation due to the polymerization of the actin filaments caused by an intracellular pH increase (Steinhardt *et al.*, 1971; Johnson and Epel, 1976; Begg and Rebhun, 1979; Tilney and Jaffe, 1980; Begg *et al.*, 1982; Yonemura and Mabuchi, 1987; Limatola *et al.*, 2021a, 2022b). Indeed, the microvilli, filled with actin filaments, impressively extend to the perivitelline space (PS; Tilney and Jaffe, 1980; Spudich *et al.*, 1988; Byrd and Belisle, 1985; Chun *et al.*, 2010; Limatola *et al.*, 2022b). Subsequently, the actin filaments in the subplasmalemmal zones undergo centripetal translocation to the inner cytoplasm (Terasaki, 1996; Limatola *et al.*, 2020a, 2020b, 2022b). At the sperm incorporation site, the fertilization cone is formed by thick actin filaments to bring the fertilizing sperm into the activated egg (Limatola *et al.*, 2021a). Therefore, the state of the cortical actin cytoskeleton of the unfertilized eggs and its remodelling after insemination determine the progressive structural and physiological changes in cortical protoplasm leading to the progressive differentiation from egg to embryo (Just, 1928).

Actin is one of the most abundant and conserved proteins in eukaryotic cells. The spatiotemporal shift of equilibrium between filamentous actin (F-actin) and monomeric globular actin (G-actin) and the consequent changes in the actin cytoskeleton play crucial roles in several biological processes within the cells, contributing to the plasticity of the cell shape, as well as cell motility, exocytosis and endocytosis, cytokinesis, and even gene regulation (Pollard and Cooper, 2009; Balasubramanian *et al.*, 2012; Hyrskyluoto and Vartiainen, 2020; Rausch and Hansen, 2020). Moreover, phosphatidylinositol(4,5)bisphosphate ( $\text{PIP}_2$ ), which is a component of the plasma membrane, not only serves as the substrate of phospholipase C (PLC) to produce the  $\text{Ca}^{2+}$ -mobilizing second messenger inositol 1,4,5-trisphosphate ( $\text{InsP}_3$ ), but also interacts with a host of actin-binding proteins and thereby modulates F-actin dynamics. Therefore,  $\text{PIP}_2$  may exemplify an intersection where the two signalling pathways meet (Yin and Janmey, 2003; Nusco *et al.*, 2006; dos Remedios and Nosworthy, 2008). Our previous studies have shown that the status of the actin filaments in the egg cortex is essential for the  $\text{Ca}^{2+}$ -linked fertilization response. As actin is a  $\text{Ca}^{2+}$ -binding protein with extremely high affinity, its polymerization and depolymerization may serve as highly efficient mechanisms for  $\text{Ca}^{2+}$  storage and release (Lange, 1999; Lim *et al.*, 2002; Chun and Santella, 2009). The polymerization status of the

subplasmalemmal actin cytoskeleton also modulates the activity of enzymes, ion channels, and other proteins involved in the sperm-induced  $\text{Ca}^{2+}$  signalling pathways (Bose and Thomas, 2009; Chun *et al.*, 2013; Vasilev *et al.*, 2018, 2021). Therefore, fine regulation of the actin filaments at the egg surface is essential for the proper fertilization response. Disturbance of the normal dynamics of the actin cytoskeleton of the unfertilized cortex of starfish and sea urchin eggs consistently affects the sperm-induced  $\text{Ca}^{2+}$  signals, induces polyspermy or inhibits sperm entry and cleavage (Puppo *et al.*, 2008; Chun *et al.*, 2014; Limatola *et al.*, 2019, 2020a, 2022a, 2023).

Given the crucial role played by the dynamic regulation of the actin cytoskeleton in the ectoplasm of echinoderm eggs, it is equally important to have a method to detect rapid changes in actin filaments with minimal disturbance. Despite its advantages, the visualization of actin filaments in intact living sea urchin eggs using microinjected fluorescent probes such as Alexa-conjugated phalloidin and LifeAct-green fluorescent protein (LifeAct-GFP) is sometimes complicated because they work by binding to F-actin. Furthermore, the visualization of rapid cortical actin changes a few seconds after fertilization during the release of  $\text{Ca}^{2+}$  and separation of the vitelline membrane may be challenged by the contraction and movement of eggs characterizing this early event. Therefore, an alternative method of visualizing actin filament changes mimicking the natural F-actin dynamics would be highly appreciated in the microscopic studies of the actin cytoskeleton. In this regard, the present study aims to apply Raman spectroscopy to monitor F-actin changes (polymerization) in sea urchin eggs following fertilization, which is well documented over several decades of studies using a fixation time series combined with light and electron microscopy. More recent work with live confocal microscopy and LifeAct-GFP microinjected into the unfertilized eggs of several different species of sea urchin has visualized actin polymerization caused by hypertonic seawater and by the fertilizing sperm (Limatola *et al.*, 2021b, 2022b), as well as in embryos (Pal *et al.*, 2020). As no fluorescent dye is necessary to bind and visually report the presence of F-actin, Raman spectroscopy might be an attractive alternative for these experimental tasks.

Raman spectroscopy is a technique based on the inelastic scattering of laser photons by vibrating molecules in the sample (Short *et al.*, 2005; Brauchle *et al.*, 2014). The energy shift of the scattered photons can be measured and displayed as a spectrum. Therefore, the relative intensity and spectral position of specific bands of the Raman spectrum provide valuable information about the biochemical composition, chemical and structural conformation, molecular interactions of the sample molecules, and their spatial distribution with minimally invasive measures (e.g. no need for microinjection of fluorescent markers). As such, Raman spectroscopy provides highly chemical-specific information on the sample, which can be interpreted for diagnostic purposes, as evidenced by previous work on cancer cell/tissue identification (Managó *et al.*, 2016; Elumalai *et al.*, 2020; Liu *et al.*, 2022; Mangini *et al.*, 2023). When a morphological change occurs in a selected cell or tissue during a biological process such as cell division, apoptosis, or stress response, this change can be identified, quantified, and visualized thanks to the consequent variation of the Raman spectrum (Short *et al.*, 2005; Brauchle *et al.*, 2014). Moreover, Raman spectroscopy has been used for studying the biochemical composition of male gametes of different mammalian species (Movasaghi *et al.*, 2007; Ferrara *et al.*, 2015a; De Angelis *et al.*, 2019; Bogliolo *et al.*, 2020) and for investigating the effect of vitrification/warming on the state of the actin cytoskeleton of sheep oocytes matured *in vitro* (Bogliolo *et al.*, 2015), as well as for monitoring the

beta-carotene granules content of sea urchin eggs (Nekvapil *et al.*, 2019). Raman spectroscopy can be applied to fixed and unfixed cells, providing biochemical information comparable and complementary to fluorescence microscopy.

In this contribution, we applied Raman spectroscopy to probe the structural changes of the actin filaments (depolymerization and polymerization) in sea urchin eggs caused by actin drugs or the fertilizing sperm. Raman maps of fixed eggs allowed the visualization of the actin cytoskeletal reorganization at different experimental conditions. These results correlated well with the fluorescent signals from living eggs microinjected with LifeAct-GFP. Therefore, Raman spectroscopy can serve as a valuable rapid and non-invasive method for evaluating F-actin dynamics that does not involve microinjection or exogenous expression but simple sample preparation.

## Materials and methods

### Gamete preparation and fertilization

*Paracentrotus lividus* samples were collected in the Gulf of Naples during the breeding season (from October to May) and maintained in circulating seawater (16°C). Artificial spawning was induced by intracoelomic injection of 0.5 M KCl. Eggs were then collected and stored in filtered seawater, while dry sperm were kept at 4°C and diluted in normal seawater (NSW pH 8.1) a few minutes before experiments. For treatments with actin drugs, eggs were treated with 3 µM latrunculin-A (LAT-A, purchased from Merck), 12 µM jasplakinolide (JAS; purchased from Molecular Probes), or 0.1% dimethyl sulphoxide (DMSO; drugs vehicle, Merck) for control eggs for 15 min at room temperature. Fertilization was performed using a final spermatozoa concentration of  $1.84 \times 10^6$  units/ml. The eggs were divided into six main groups: Unfertilized (eggs in seawater not inseminated), 15 s pf (eggs 15 s after insemination), 15 min pf (eggs 15 min after insemination), Control (DMSO) (untreated eggs exposed to DMSO for 15 min), LAT-A (eggs treated with LAT-A for 15 min), and JAS (eggs exposed to JAS for 15 min).

### Microinjection and live cell imaging

Living *P. lividus* eggs were microinjected with 5 mg/ml of bacterially expressed LifeAct-GFP fusion protein (a generous gift from A. McDougall of UPMC Sorbonne University, France) using an air pressure transjector (Eppendorf FemtoJet, Hamburg, Germany). The extracellular layers of the eggs were left intact without preliminary treatment, as previously described (Chun *et al.*, 2014). The visualization of the cortical F-actin structure and its dynamics at fertilization was observed by a Leica TCS SP8X inverted confocal laser scanning microscope equipped with a white light laser and hybrid detectors (Leica Microsystems, Wetzlar, Germany). Fluorescence images were collected on the confocal microscope to quantify the LifeAct-GFP signals representing F-actin on the confocal plane. A MetaMorph scan was performed to obtain the mean of the fluorescence intensity along the line.

### Raman spectroscopy analysis and sample preparation

Aliquots of eggs were fixed before and after fertilization (15 s and 15 min after insemination) with 2% paraformaldehyde for 20 min at room temperature. Samples were washed twice in seawater and stored at 4°C until Raman spectroscopy analysis was performed. Raman spectra were collected using an inverted confocal Raman

microscope (XploRA INV, Horiba Jobin Yvon, Villeneuve d'Ascq, France) equipped with a 532 nm wavelength diode laser (laser power = sample 2 mW) and a X60 water immersion objective (Nikon, Ti-2000 Eclipse, Nikon Instruments Europe BV, Amsterdam, Netherlands, Numerical aperture (NA) = 1.2). The excitation laser wavelength and intensity were selected to avoid any possible phototoxic effect on the cells (Ferrara *et al.*, 2015b).

The scattered light from the sample was spectrally filtered by a holographic notch filter, then spatially filtered by a pinhole (300 µm), and finally directed to the spectrometer, equipped with a 600 lines/mm holographic grating. The Raman scattered light was focused into the spectrometer entrance slit (100 µm) and imaged using a thermoelectrically cooled charge-coupled device (CCD) camera.

Fixed eggs in NSW were sandwiched between two CaF<sub>2</sub> coverslips and then sealed with standard nail polish. Each Raman spectrum was acquired with an integration time of 1 s. Spectra were normalized by subtracting the solvent background signal followed by an additional baseline correction. Data were analyzed using Origin software. Mean Raman spectra of the egg cortex were generated using 500 spectra (50 for each sample) acquired in the outer cytoplasmic region of the eggs (~6–7 µm from the external egg edge) in the fingerprint region (between 1000–1800 cm<sup>-1</sup>) and CH region (between 2800–3000 cm<sup>-1</sup>). The spectrum Raman intensities were normalized by the maximum peak intensity and reported in arbitrary units. The analysis was repeated on 10 cells ( $n = 10$ ) per each experimental condition. The actin Raman spectrum was obtained by analyzing in reference to the purified actin commercially available (Sigma Aldrich).

The Raman image was recorded using raster scanning over a selected cell region through the laser focus with a step size of 0.5 µm. Univariate intensity maps were constructed by integrating the Raman spectral region corresponding to F-actin (for instance, the band at 1440 cm<sup>-1</sup>) using the Horiba Scientific Laboratory Spec 6 software (Horiba Jobin Yvon, Villeneuve d'Ascq, France) (Managó *et al.*, 2018). The spectra used for the imaging map were baseline and cosmic ray corrected.

## Results

### Visualization of the actin filaments in living sea urchin eggs by use of microinjected LifeAct-GFP

To define the structural changes of the actin cytoskeleton in sea urchin eggs following the treatment with actin drugs or fertilizing sperm, intact *P. lividus* eggs were microinjected with LifeAct-GFP and exposed to 3 µM LAT-A, 12 µM JAS, or sperm. These two drugs were chosen because they induce F-actin depolymerization and polymerization, respectively. After incubation at certain intervals, the fluorescence images representing F-actin were analyzed using confocal microscopy (Figure 1). As expected, the control eggs, Control (DMSO), treated only with the drug vehicle 0.1% DMSO, ( $n = 3$ ) displayed signals at the subplasmalemmal region where dense meshwork of actin filaments are located (Figure 1a).

Following the exposure to LAT-A (3 µM, 15 min), which disrupts microfilament organization by inhibiting actin assembly, net depolymerization of actin filaments was most notable at the subplasmalemmal region of the eggs ( $n = 3$ ). As shown in the line scanning profiles of the confocal plane (Figure 1A, lower panel), the two sharp peaks of the signals coming from the subplasmalemmal regions are eliminated by the drug treatment, indicating



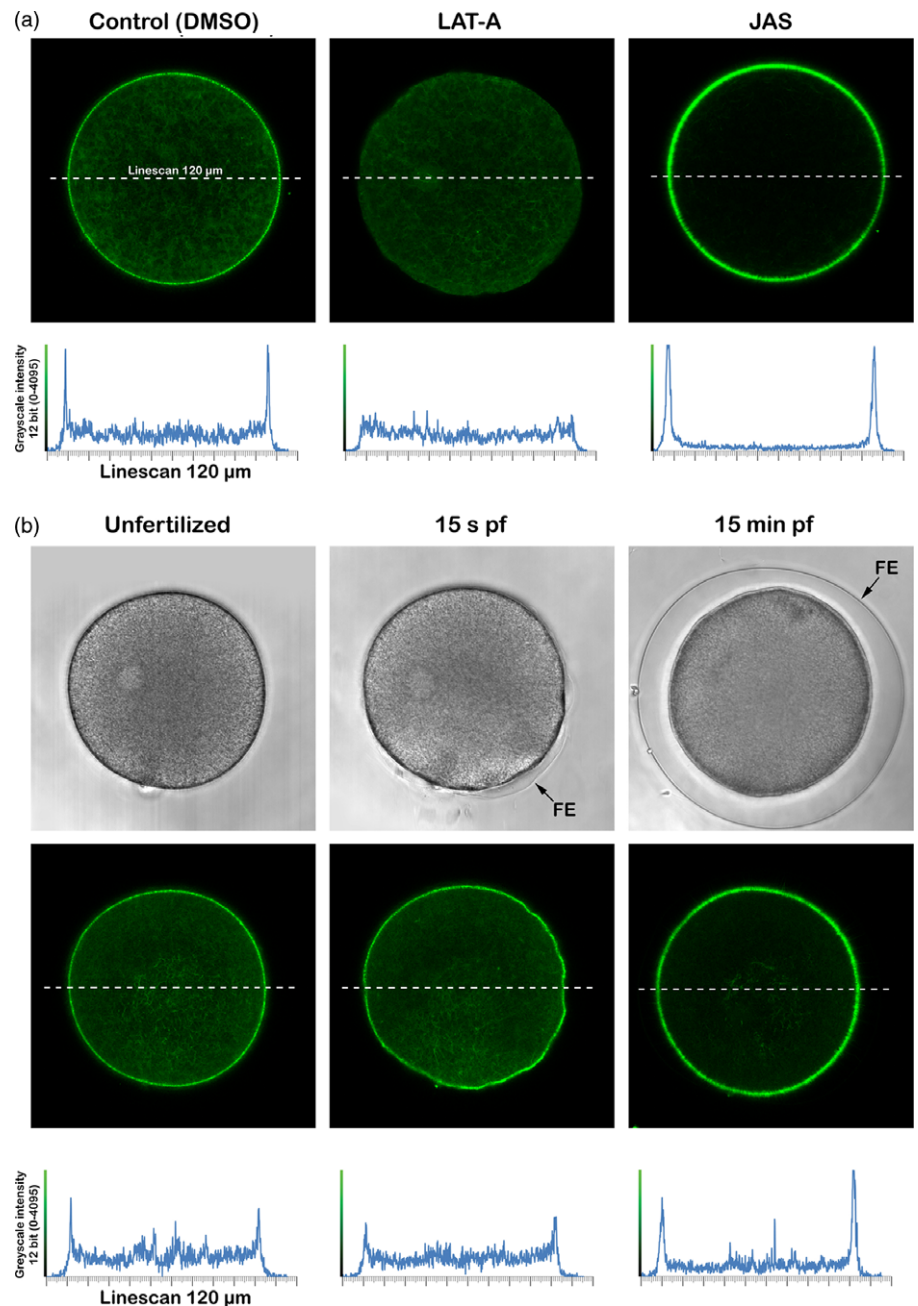


**Figure 1.** Visualization of the actin filaments in live sea urchin eggs using microinjected LifeAct-GFP. Intact *P. lividus* eggs were microinjected with 5  $\mu\text{g}/\mu\text{l}$  (pipette concentration) of LifeAct-GFP 10 min before various treatments. (a) Incubation with actin drugs for 15 min: Control (0.1% DMSO, vehicle of the drug), LAT-A (3  $\mu\text{M}$ ), and JAS (12  $\mu\text{M}$ ). (b) Fertilization: Control (unfertilized), 15 s after fertilization (15 s pf), and 15 min after fertilization (15 min pf). F-actin (green) confocal images were captured and quantified by MetaMorph line scanning across the confocal plane (dotted lines). The length of the line-scan path is 120  $\mu\text{m}$ . Note the initiation of the fertilization envelope formation by 15 s after insemination and its total elevation by 15 min later (B, transmitted light view on the upper panel). Abbreviations: FE, fertilization envelope; JAS, jasplakinolide; LAT-A, latrunculin-A; pf, post-fertilization.

that this subcellular region is most active in actin tread-milling at the resting condition. Conversely, a similar treatment with JAS (12  $\mu\text{M}$ , 15 min), which stabilized actin filaments, produced a net increment of the F-actin signals (Figure 1a) at the subplasmalemmal regions of the eggs ( $n=3$ ). Interestingly, the hyperpolymerization of actin filaments near the plasma membrane of these eggs caused the overall depletion of the actin pools in all other areas, as judged by the striking reduction of the fluorescent signals in the profile of line scanning at the regions representing the inner cytoplasm (Figure 1a, lower panel).

Following fertilization, conversely, the eggs ( $n=4$ ) also exhibited notable changes in the distribution of F-actin over the confocal plane (Figure 1b). By 15 s after fertilization, F-actin visualized in the tight subplasmalemmal zone of the same egg before insemination was appreciably reduced, as judged by the

amplitude of the fluorescent signals emitted by LifeAct-GFP in the region (Figure 1b). At 15 s after fertilization, which is the time during which a  $\text{Ca}^{2+}$  increase is concomitant with the initiation of the elevation of the FE, less actin filaments are visible in the cortical area except for the core region of the zygote (Figure 1b lower panel, see also Figure 3c). By contrast, at 15 min after fertilization, subplasmalemmal F-actin meshwork becomes dense again, as judged by the amplitude of the fluorescent signals reported by LifeAct-GFP in that region (Figure 1b). Both in fertilized eggs and in the eggs treated with JAS, it may be noteworthy that the F-actin signals in the subplasmalemmal area are not uniform, but preferentially denser on one side compared with the other. This result is not likely to be related to a margin of error in microinjection (e.g. the signals in the unfertilized eggs are relatively uniform) but may reflect the cytoskeletal asymmetry

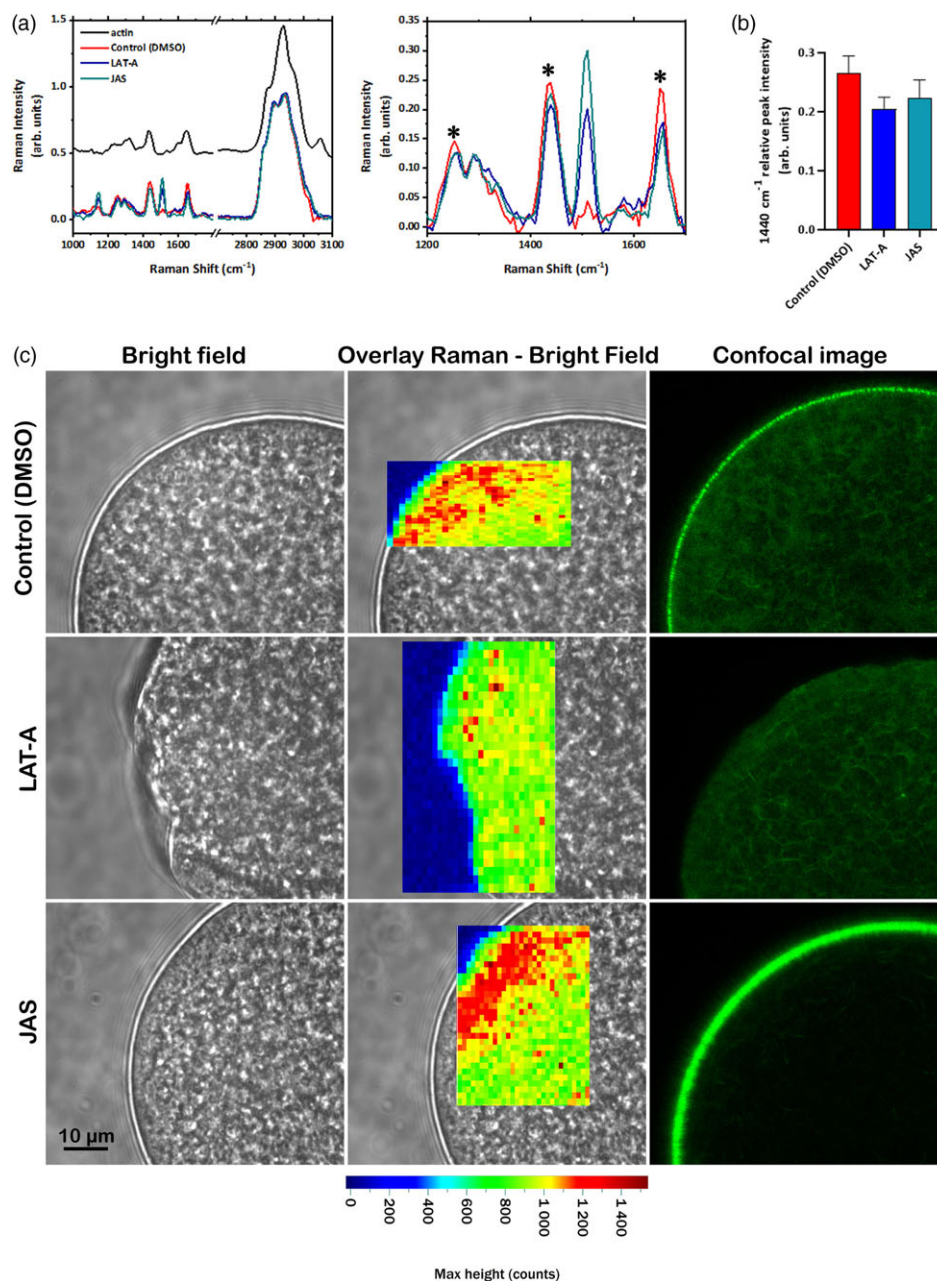


**Figure 2.** Raman spectroscopic evaluation of the F-actin distribution before and after exposure of sea urchin eggs to actin drugs. *P. lividus* eggs were fixed after the bath incubation with 0.1% DMSO (control), 3  $\mu$ M LAT-A, or 12  $\mu$ M JAS for 15 min, and subjected to Raman spectroscopy. For comparison, the distribution of F-actin was examined using confocal fluorescence microscopy in living eggs pre-injected with LifeAct-GFP under the same conditions. (a) Raman spectra of actin (black line), control (DMSO, red line), LAT-A (blue line), and JAS-treated eggs (green line). The zoomed profile of the spectra in the region from 1200 to 1700  $\text{cm}^{-1}$  is shown in the right panel. Data are presented as a mean of 500 spectra (50 for each sample) acquired from sea urchin eggs ( $n = 10$ ). Asterisks indicate the peaks that changed their intensity and/or shapes under treatment with the actin-binding drugs. The spectra are horizontally shifted. (b) Histogram showing the relative intensity of the 1440  $\text{cm}^{-1}$  peak in the normalized spectra of Control (DMSO), LAT-A and JAS-treated eggs. The data are shown as mean  $\pm$  SDs of 500 spectra (50 spectra for each sample, 10 eggs for experimental condition). (c) Representative eggs in each experimental condition were visualized by brightfield (left panel), and Raman imaging (middle panel). The Raman map was obtained by plotting the intensity of the 1440  $\text{cm}^{-1}$  peak (Amides I and III). The same intensity scale (in photon counts) has been used for all the maps. Eggs in the same experimental condition, analyzed using LifeAct-GFP by confocal fluorescence microscopy, were additionally shown for comparison (right panel).

linked to the egg polarity constantly enhanced when actin undergoes polymerization following fertilization and after JAS treatment (Limatola *et al.*, 2019).

#### Raman spectroscopic assessment of F-actin changes in the eggs treated with actin drugs

Label-free Raman spectroscopy was used for assessing the structural changes in the actin cytoskeleton of sea urchin eggs after the treatment with two actin drugs LAT-A and JAS. Following the procedure described in the Materials and Methods, the 500 Raman spectra, 50 spectra per egg ( $n = 10$ ), were acquired from the subplasmalemmal region of the egg,  $\sim 6\text{--}7\text{ }\mu\text{m}$  from the egg's surface, where the most significant F-actin changes occur during fertilization. The spectrum Raman intensities were normalized by maximum peak intensity (band at 2930  $\text{cm}^{-1}$ ) to emphasize the relative variation of specific Raman bands. These normalized

spectra cannot provide information on the concentration/distribution of the cortical actin cytoskeleton but on the spectrum modification due to the drugs.

The average Raman spectra of untreated eggs, Control (DMSO), and those treated with LAT-A or JAS were then analyzed at the fingerprint region (1000–1800  $\text{cm}^{-1}$ ). As a reference, the normalized spectrum of purified actin is also shown (Figure 2A). The mean spectra from the eggs mainly contained bands related to proteins and lipids: aromatic ring vibration of amide III at 1253  $\text{cm}^{-1}$  and 1291  $\text{cm}^{-1}$  (C–N stretch, N–H bend),  $\text{CH}_2$  vibrations of aliphatic side chains 1440  $\text{cm}^{-1}$  and amide I at 1652  $\text{cm}^{-1}$  (Movasaghi *et al.*, 2007). These bands were also visible in the spectral profile of the purified actin (black line in Figure 2a). Moreover, the egg spectra also contained the characteristic bands typically associated with carotenoids, i.e. the peaks at 1150  $\text{cm}^{-1}$  and 1508  $\text{cm}^{-1}$  (Nekvapil *et al.*, 2019). The higher frequency region was characterized by the two bands between 2895 and 2930  $\text{cm}^{-1}$

that were assigned to the  $\text{CH}_3$  and  $\text{CH}_2$  symmetric stretch of lipids, which was not visible in the spectra of purified actin. The band at  $2895\text{ cm}^{-1}$  was assigned to the  $\text{CH}_2$  asymmetric stretch, and the one at  $2930\text{ cm}^{-1}$  to the  $\text{CH}$  stretch. Both bands contained contributions from lipids and proteins and were visible with different relative intensities in the spectra of eggs and purified actin.

By comparing the spectra of the control eggs and those treated with the actin drugs normalized to the highest lipid band, it is possible to highlight the variations in the fingerprint spectral regions. Overall, most spectral peaks were shared by actin and control eggs, indicating that actin is the major component of the subplasmalemmal region. In the spectral profiles of the eggs treated with the two drugs, the intensity, and shape of the bands were mainly changed in the spectral regions at  $\sim 1253$ ,  $1291$ ,  $1440$ , and  $1652\text{ cm}^{-1}$ , which precisely correspond to the areas of the secondary protein structure, namely, amide I, amide III and C–C stretching regions (Figure 2b; Roessl *et al.*, 2014). These spectral changes indicated that the drugs induced a change in the vibration characters of the protein, as actin forms a more disordered structure (Zeng *et al.* 1997). This effect was particularly evident for the band at  $1440\text{ cm}^{-1}$ , as shown in Figure 2b. Therefore, these Raman spectral peaks could serve as useful physical ‘markers’ to monitor the cortical actin cytoskeletal changes in a label-free way. In the eggs treated with LAT-A or JAS, the band intensity is also markedly strong at  $1150\text{ cm}^{-1}$  and  $1508\text{ cm}^{-1}$ . This shift at the bands, which are characteristic of carotenoids but are nearly absent in the spectra of purified actin, is probably due to a mechanical rearrangement of the whole cortical structure of the eggs, which affects the relocation of the carotenoid granules rather than the actin cytoskeletal changes directly related to the protein structure.

For spatial localization of the actin rearrangement and reconstruction of false colour Raman maps, the Amide I and III bands at  $1440\text{ cm}^{-1}$  were analyzed in the control (DMSO), LAT-A- and JAS-treated eggs (Figure 2c). Indeed, as previously reported (Bogliolo *et al.*, 2015), this band which was used to identify changes in the cortical F-actin network of *in vitro* matured ovine oocytes following exposure to cryoprotectants and vitrification, showed marked relative intensity changes in sea urchin eggs after the treatment with the actin drugs (Figure 2c). The colour scale bar indicates the absolute intensity of the  $1440\text{ cm}^{-1}$  band (in photon counts) in Figure 2C and all other Raman maps in this study. For the control eggs, high actin clustering was observed in the cortical region, and this effect was more evident in JAS-treated eggs, suggesting a more compact rearrangement of actin. As for the LAT-A-treated eggs, the Raman spectrum is less intense, probably due to cortical actin depolymerization and the signal of the  $1440\text{ cm}^{-1}$  band being more delocalized compared with the control eggs. When Raman maps were compared with confocal fluorescence analysis with Life-Act-GFP staining performed in the three experimental conditions (Control, LAT-A- and JAS-treated eggs), there was a good agreement between the results obtained by the two methods. This observation validates the use of Raman imaging and the band at  $1440\text{ cm}^{-1}$  for label-free assessment of the cortical actin cytoskeleton changes, as exemplified by the fixed eggs pretreated with LAT-A and JAS, which depolymerizes and hyperpolymerizes actin, respectively.

#### Raman spectroscopic assessment of F-actin changes in the fertilized eggs

Sea urchin eggs (*P. lividus*) were fertilized and fixed 15 s and 15 min after insemination and subsequently analyzed using Raman

spectroscopy (Figure 3a). The average spectra collected from the cortical region of the eggs before and after fertilization exhibited the expected results analogous to those observed with LAT-A- and JAS-treated eggs. Therefore, the spectral bands at  $\sim 1253$ ,  $1440$ , and  $1652\text{ cm}^{-1}$ , mainly associated with Amide I and Amide III, altered relative intensity during fertilization. After 15 s of sperm addition, a significant change of the bands at  $1253\text{ cm}^{-1}$  was similar to the observation in the eggs treated with LAT-A-treated eggs (Figure 2b), suggesting depolymerization of the F-actin. Moreover, spectral changes are accompanied by a substantial shift of the carotenoid band at  $1150\text{ cm}^{-1}$ , which was also observed in the eggs treated with actin drugs. Therefore, the consistent alteration of the Raman spectral patterns in the fertilized eggs suggests that both the actin cytoskeleton and carotenoid-rich granules are being reorganized in the cortex in a manner comparable with the eggs treated with the actin drugs. For example, 15 min after fertilization, there was a reduction of the intensity of the bands at  $1440$  and  $1652\text{ cm}^{-1}$  (Figure 3b), which is similar to the decrease in JAS-treated eggs (Figure 2b), suggesting a hyperpolymerization of the F-actin. Altogether, these results indicate that the actin polymerization status and the protein aggregation and reorganization can be monitored by Raman spectroscopy in a label-free way during sea urchin egg fertilization.

The spectral analysis demonstrated that the Amide I and III bands at  $1253$ ,  $1440$ , and  $1652\text{ cm}^{-1}$ , mainly associated with the F-actin structure, were specifically modulated after fertilization and LAT-A- or JAS treatments. Therefore, we used these spectral bands to monitor the spatial rearrangements of the egg cortex following fertilization. For comparison, intact eggs ( $n = 4$ ) pre-injected with LifeAct-GFP were fertilized, and the distribution of F-actin was analyzed by live cell imaging confocal microscopy at the same time points (Figure 3c). In the cortical region, the Raman map obtained by plotting the intensity of the band at  $1440\text{ cm}^{-1}$ , showed a less intense signal, reflecting the disturbed distribution of actin filaments 15 s after the insemination. This change and the spectral analysis suggest F-actin depolymerization in the fertilized egg cortex in the early phase of egg activation comprising the measured intracellular  $\text{Ca}^{2+}$  release, as confirmed by fluorescence imaging of the actin visualization. After 15 min from the fertilization, the Raman map shows a more compact actin rearrangement. Therefore, this change and the spectroscopic analysis can be interpreted as cortical actin hyperpolymerization and the formation of the dense actin meshwork, further confirmed by confocal fluorescence microscopy (Figure 3C).

#### Discussion

It is widely accepted that the correct development of mammalian embryos after fertilization relies on the quality of gametes, particularly the female ones (Movasaghi *et al.*, 2007). Devising a non-invasive method to evaluate the quality of oocytes and eggs is one of the significant objectives in embryology and in the practice of assisted reproductive technologies because it will enhance the success rate of reproduction in both medical and veterinary fields. Quality control of oocytes and eggs is usually performed considering morphological criteria. Still, this method needs to be more accurate because the morphology of a cell often does not reflect its quality. For this reason, oocytes and eggs need to be subjected to more invasive analysis to obtain more structural and biochemical information that ensures gamete quality. In particular, one of the most decisive characteristics is the state of the actin cytoskeleton. It is indeed well known that the quality of oocytes and



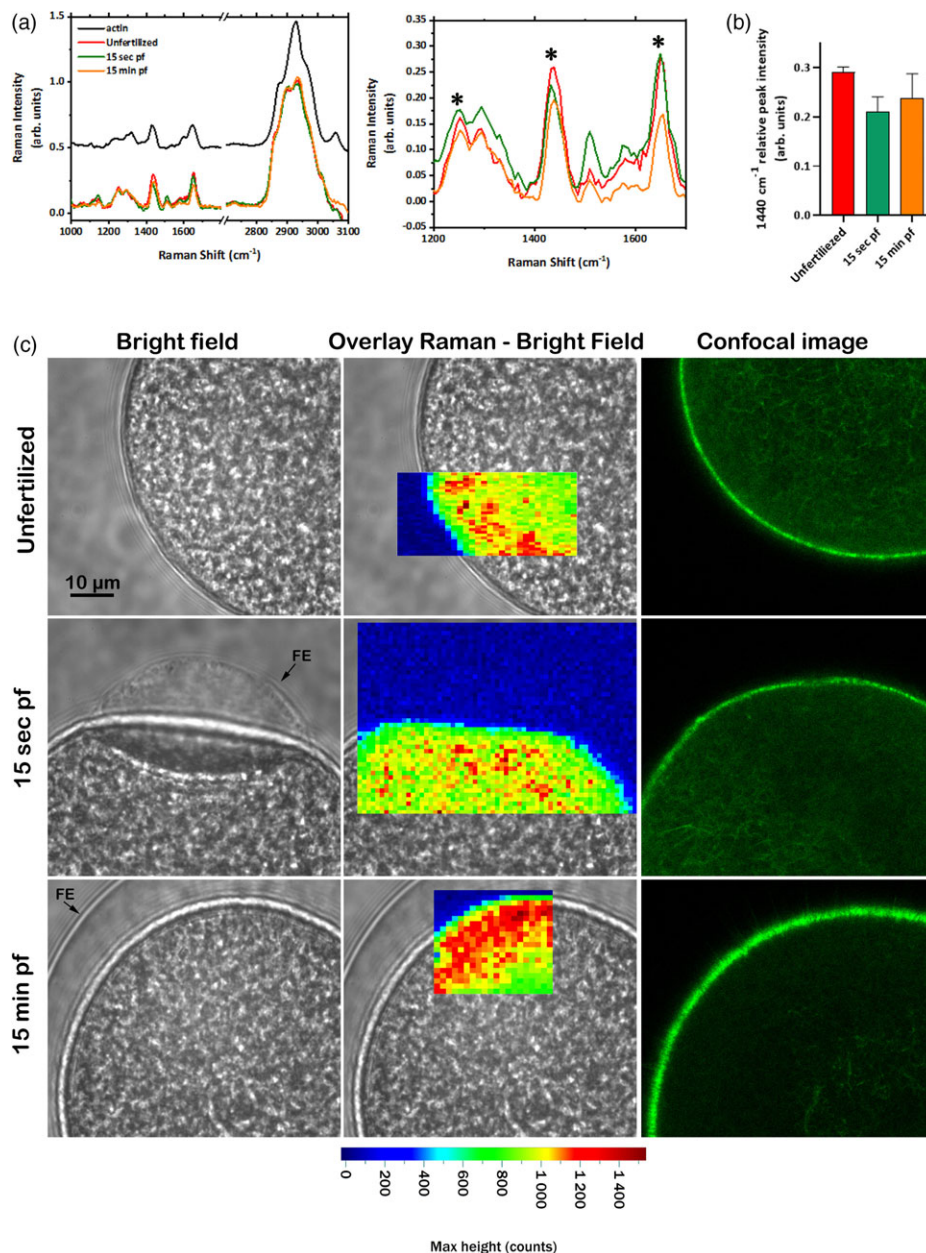


**Figure 3.** Raman spectroscopic evaluation of the F-actin distribution and its changes in fertilized eggs of sea urchin *P. lividus* eggs were fixed before or after fertilization (15 s or 15 min) and subjected to Raman spectroscopy. For comparison, the distribution of F-actin was examined by conventional confocal microscopy in live eggs pre-injected with LifeAct-GFP. (a) Results of Raman spectra at each time interval. Spectral profiles: Raman spectra of purified actin (black line); unfertilized (red line); fertilized eggs after 15 s (green line); fertilized eggs after 15 min (orange line). The panel on the right represents the zoomed spectra in the region from 1200 to 1700 cm<sup>-1</sup>. Data are presented as a mean  $\pm$  standard deviation (SD) of 500 spectra (50 for each sample) acquired from sea urchin eggs ( $n = 10$ ), normalized by the highest band. Asterisks indicate the peaks that changed their relative intensity and/or shapes after fertilization. The spectra are horizontally shifted. (b) Graph showing the relative intensity of the 1440 cm<sup>-1</sup> peak in the normalized spectra of unfertilized, 15 s and 15 min after fertilization. The data are presented as the mean  $\pm$  standard deviation (SD) of 500 spectra. (c) Representative eggs in each experimental condition were visualized by brightfield (left panel), Raman (middle panel), and confocal fluorescence microscopy (right panel). The Raman map was obtained by plotting the intensity of the 1440 cm<sup>-1</sup> peak. Abbreviations: FE, fertilization envelope; pf, post-fertilization.

eggs strictly relies on the structure and function of the actin cytoskeleton because it plays a central role during oocyte maturation, oocyte polarity control, and the fertilization process (Maro *et al.*, 1984; Terada *et al.*, 2005; Li and Albertini, 2013; Lee *et al.*, 2014). In particular, the changes in the actin cytoskeleton dynamics in fertilized eggs of sea urchins have been traditionally investigated for decades, mainly by light and electron microscopy observations of fixed samples. The latter provided a high resolution at the ultrastructural level of the organization of the actin filaments before and following fertilization (Begg and Rebhun, 1979; Begg *et al.*, 1982; Henson and Begg, 1988).

Recent live cell experiments with confocal microscopy conducted in our laboratory using different fluorescent actin probes microinjected into unfertilized eggs have visualized two different cortical actin pools. Specifically, an actin ring immediately beneath the egg plasma membrane is more prominently visualized by LifeAct-GFP than by Alexa-Phalloidin, which starts

to undergo polymerization 5 min after insemination (Limatola *et al.*, 2022b; this contribution). Conversely, actin filaments translocating from the cortical region to the centre of the fertilized egg are more efficiently visualized by AlexaPhalloidin (Limatola *et al.*, 2020a, 2020b, 2021a, 2022b). In addition, the fact that the actin fibres oriented perpendicularly to the surface of a mature egg of starfish (Santella and Chun, 2022) was not observed in living sea urchin eggs and suggests the diverse morpho-functionality of the egg cortex of the two echinoderm species that are fertilized at different meiotic stages (Just, 1939). The morpho-functional status of the actin filaments also depends on experimental conditions. Obviously, live intact cells without much manipulation are closer to their natural physiological conditions compared with isolated cortices, often utilized in ultrastructural studies (Sardet, 1984; Henson and Begg, 1988). The crucial role of the structural organization of the actin of the cortex of unfertilized eggs in controlling a series of fast and slow events triggered by sperm

stimulation has been amply demonstrated. They include sperm-egg interaction,  $\text{Ca}^{2+}$  signals starting a few seconds after insemination, CG exocytosis, and the associated lifting of the FE. To these early events, the cortical actin polymerization encompassing microvilli elongation follows in preparation of sperm entry and cleavage (Limatola *et al.*, 2020b, 2021b, 2022a, 2022b). Indeed, if the cytoskeletal structure of the egg cortex is altered before insemination, binding and fusion with spermatozoa and the subsequent  $\text{Ca}^{2+}$  signalling go astray, resulting in polyspermy or failure of sperm entry. Even for monospermy, the prior alteration of the cortical actin cytoskeleton of the unfertilized eggs also compromises the subsequent embryonic development (Limatola *et al.*, 2019). However, even if the live cell imaging methods with fluorescent compounds have the advantage of providing information on the structural dynamics of the actin of intact eggs in experimental conditions that recapitulate what happens at sea, their application still requires considerable individual technical skills. For these reasons, a non-invasive method that quickly enables the visualization and structural identification of the actin cytoskeleton changes without cell labelling would be highly desirable. Therefore, in the present communication, we applied Raman spectroscopy and imaging to detect the changes in the actin cytoskeleton in sea urchin eggs during the physiological response (early and late phases of the fertilization process) and following pharmacological treatments (LAT-A and JAS). The treatment with LAT-A and JAS affects actin peaks at 1253, 1291, 1440, and 1652  $\text{cm}^{-1}$  of the Raman spectrum. Indeed, these peaks have already been associated with actin changes in sheep oocytes (Bogliolo *et al.*, 2015). The subtle spectral changes observed in these peaks compared with the spectral profile of purified actin are likely to reflect the conformation of the protein induced by depolymerization or hyperpolymerization of actin in the subplasmalemmal zone. By plotting the intensity of the band at 1440  $\text{cm}^{-1}$ , showing the most important modulation, it was possible to visualize the actin cytoskeleton rearrangement during sea urchin eggs before and after pharmacological treatment. Indeed, in the cortical region of the control eggs, it manifested high actin concentration, and this effect was even more evident in JAS-treated eggs, suggesting a more compact rearrangement of the actin in the latter case (F-actin hyperpolymerization). Due to actin depolymerization, the actin Raman signal was less intense and more delocalized for the LAT-A-treated eggs. The reconstructed Raman maps were in very good agreement with confocal fluorescence images, confirming that the intensity of the band at 1440  $\text{cm}^{-1}$  could be used for studying actin localization.

A substantial increase in the hallmark bands of carotenoids was observed after the LAT-A and JAS and was attributed to the secondary changes inflicted on the organization of the vesicles in the egg cortex, which are rich in carotenoids (Roessl *et al.*, 2014). Indeed, the actin cytoskeleton is involved in rearranging the whole cortical structure of the eggs by mobilizing vesicles. In doing so, carotenoid granules may be relocated, and their protein component may be indirectly affected by their vibration kinetics.

The spectral results have shown a similar structural change of the F-actin after fertilization, *i.e.*, relative intensity variation of the actin Raman bands and Raman imaging allowed identification of the actin depolymerization 15 s after and polymerization 15 min after insemination ( $n = 10$ ). After 15 s from fertilization, the Raman maps show that actin filament signals are less intense and uniformly distributed in the egg cortex, resembling the distribution obtained after LAT-A treatment. Instead, 15 min after insemination, actin was polymerized at the egg cortex, where

F-actin forms a very dense layer under the plasma membrane. Therefore, the Raman images correlated reasonably well with the LifeAct-GFP signals of F-actin in living eggs.

The main issue of detecting actin disassembly in eggs 15 s after sperm addition was rather challenging due to the movement and contraction of the fertilized eggs that undergo separation of the vitelline layer from the egg plasma membrane following the exocytosis of the content of CG into the PS (Figure 3). The actin depolymerization in the fertilized egg cortex which coincides with the early  $\text{Ca}^{2+}$  release event is followed by actin polymerization during the late phase of egg activation, starting 5 min after insemination, as shown previously (Limatola *et al.*, 2022b). The results of this contribution demonstrated that the characteristic changes of the Raman spectral peaks in the eggs fixed 15 s and 15 min after insemination were comparable with the cortical actin depolymerization and polymerization phases scarcely visualized by injected LifeAct-GFP. Compared with confocal fluorescence microscopy or other microscopy techniques, Raman microscopy may provide a lower spatial resolution but allow biochemical identification of the actin 'status.'

Even if we had used fixed samples for Raman analysis, it is worth mentioning that the excitation laser's wavelength and intensity had been selected to avoid any possible phototoxic effect on the cells. We have not evaluated directly if the laser-irradiated zygotes develop normally; further analysis is required to confirm this point. However, the data reported by Perevedentseva *et al.* (2019) confirm that we had selected safe parameters for the living embryo measurements.

Label-free Raman imaging of eggs treated with drugs or fertilized at two different times has been used to correlate the biochemical and morphological information. Therefore, it can be used in correlation with standard imaging protocols for analyzing samples with no or minimal manipulation and, therefore, for exploring the samples in the most physiological possible condition to avoid data misinterpretation.

In conclusion, our work has shown that Raman spectroscopy could help to monitor the actin cytoskeletal modifications during fertilization without microinjecting fluorescent probes. Nonetheless, it bears an emphasis that the new approach based on this technique may detect subtle changes that are often very difficult to resolve in confocal microscopy using living eggs due to the rapid morphological changes of the actin filaments that it was easier to capture using fixed samples. Therefore, each method supplements the other.

**Acknowledgements.** The authors thank Davide Caramiello from CAPE Department for maintaining sea urchins in the tanks and Giovanni Gragnaniello and Stefano Managó for helping to prepare the figures.

**Financial support.** This research received no specific grant from public, commercial, or non-profit funding agencies. It was financially supported by institutional funds (fellowship) the Stazione Zoologica Anton Dohrn granted to N.L. M.M. is supported by a PON IMPARA fellowship. The authors thank the POR CIRO infrastructure and Euro-Bioimaging for Raman imaging.

**Competing interests.** The authors declare no conflict of interest.

**Ethical standard.** Sea urchins (*Paracentrotus lividus*) used for the present study were collected according to the Italian legislation (DPR 1639/68, 19 September 1980 and confirmed on 1 October 2000). All the experimental procedures were carried out following the guidelines of the European Union (Directive 609/86).



## References

- Balasubramanian, M. K., Srinivasan, R., Huang, Y. and Ng, K. H. (2012). Comparing contractile apparatus-driven cytokinesis mechanisms across kingdoms. *Cytoskeleton*, **69**(11), 942–956. doi: [10.1002/cm.21082](https://doi.org/10.1002/cm.21082)
- Begg, D. A. and Rebhun, L. I. (1979). pH regulates the polymerization of actin in the sea urchin egg cortex. *Journal of Cell Biology*, **83**(1), 241–248. doi: [10.1083/jcb.83.1.241](https://doi.org/10.1083/jcb.83.1.241)
- Begg, D. A., Rebhun, L. I. and Hyatt, H. (1982). Structural organization of actin in the sea urchin egg cortex: Microvillar elongation in the absence of actin filament bundle formation. *Journal of Cell Biology*, **93**(1), 24–32. doi: [10.1083/jcb.93.1.24](https://doi.org/10.1083/jcb.93.1.24)
- Bogliolo, L., Murrone, O., Piccinini, M., Ariu, F., Ledda, S., Tilocca, S. and Albertini, D. F. (2015). Evaluation of the impact of vitrification on the actin cytoskeleton of *in vitro* matured ovine oocytes by means of Raman microspectroscopy. *Journal of Assisted Reproduction and Genetics*, **32**(2), 185–193. doi: [10.1007/s10815-014-0389-7](https://doi.org/10.1007/s10815-014-0389-7)
- Bogliolo, L., Leoni, G. G. and Ledda, S. (2020). Raman spectroscopy-based approach to study the female gamete. *Theriogenology*, **150**, 268–275. doi: [10.1016/j.theriogenology.2020.01.059](https://doi.org/10.1016/j.theriogenology.2020.01.059)
- Bose, D. D. and Thomas, D. W. (2009). The actin cytoskeleton differentially regulates NG115-401L cell ryanodine receptor and inositol 1,4,5-trisphosphate receptor induced calcium signaling pathways. *Biochemical and Biophysical Research Communications*, **379**(2), 594–599. doi: [10.1016/j.bbrc.2008.12.138](https://doi.org/10.1016/j.bbrc.2008.12.138)
- Brauchle, E., Thude, S., Brucker, S. Y. and Schenke-Layland, K. (2014). Cell death stages in single apoptotic and necrotic cells monitored by Raman microspectroscopy. *Scientific Reports*, **4**, 4698. doi: [10.1038/srep04698](https://doi.org/10.1038/srep04698)
- Byrd, W. and Belisle, B. W. (1985). Microvillar elongation following parthenogenetic activation of sea urchin eggs. *Experimental Cell Research*, **159**(1), 211–223. doi: [10.1016/s0014-4827\(85\)80050-1](https://doi.org/10.1016/s0014-4827(85)80050-1)
- Chiba, K. (2020). Oocyte maturation in starfish. *Cells*, **9**(2). doi: [10.3390/cells9020476](https://doi.org/10.3390/cells9020476)
- Chun, J. T. and Santella, L. (2009). Roles of the actin-binding proteins in intracellular  $\text{Ca}^{2+}$  signalling. *Acta Physiologica (Oxford, England)*, **195**(1), 61–70. doi: [10.1111/j.1748-1716.2008.01921.x](https://doi.org/10.1111/j.1748-1716.2008.01921.x)
- Chun, J. T., Puppo, A., Vasilev, F., Gragnaniello, G., Garante, E. and Santella, L. (2010). The biphasic increase of  $\text{PIP}_2$  in the fertilized eggs of starfish: New roles in actin polymerization and  $\text{Ca}^{2+}$  signaling. *PLOS ONE*, **5**(11), e14100. doi: [10.1371/journal.pone.0014100](https://doi.org/10.1371/journal.pone.0014100)
- Chun, J. T., Vasilev, F. and Santella, L. (2013). Antibody against the actin-binding protein depactin attenuates  $\text{Ca}^{2+}$  signaling in starfish eggs. *Biochemical and Biophysical Research Communications*, **441**(2), 301–307. doi: [10.1016/j.bbrc.2013.09.103](https://doi.org/10.1016/j.bbrc.2013.09.103)
- Chun, J. T., Limatola, N., Vasilev, F. and Santella, L. (2014). Early events of fertilization in sea urchin eggs are sensitive to actin-binding organic molecules. *Biochemical and Biophysical Research Communications*, **450**(3), 1166–1174. doi: [10.1016/j.bbrc.2014.06.057](https://doi.org/10.1016/j.bbrc.2014.06.057)
- Chun, J. T., Vasilev, F., Limatola, N. and Santella, L. (2018). Fertilization in starfish and sea urchin: Roles of actin. *Results and Problems in Cell Differentiation*, **65**, 33–47. doi: [10.1007/978-3-319-92486-1\\_3](https://doi.org/10.1007/978-3-319-92486-1_3)
- De Angelis, A., Ferrara, M. A., Coppola, G., Di Matteo, L., Siani, L., Dale, B., Coppola, G. and De Luca, A. C. (2019). Combined Raman and polarization sensitive holographic imaging for a multimodal label-free assessment of human sperm function. *Scientific Reports*, **9**(1), 4823. doi: [10.1038/s41598-019-41400-0](https://doi.org/10.1038/s41598-019-41400-0)
- dos Remedios, C. G. and Nosworthy, N. J. (2008). The role of  $\text{PIP}_2$  in actin, actin-binding proteins and disease. In: dos Remedios, C. G., Chhabra, D. (eds) *Actin-Binding Proteins and Disease*. Protein Reviews, vol 8. Springer, New York, NY. pp. 290–297. doi: [10.1007/978-0-387-71749-4\\_12](https://doi.org/10.1007/978-0-387-71749-4_12)
- Elumalai, S., Managó, S. and De Luca, A. C. (2020). Raman microscopy: Progress in research on cancer cell sensing. *Sensors*, **20**(19). doi: [10.3390/s20195525](https://doi.org/10.3390/s20195525)
- Epel, D. (1978). Mechanisms of activation of sperm and egg during fertilization of sea urchin gametes. *Current Topics in Developmental Biology*, **12**, 185–246. doi: [10.1016/s0070-2153\(08\)60597-9](https://doi.org/10.1016/s0070-2153(08)60597-9)
- Epel, D., Weaver, A. M. and Mazia, D. (1970). Methods for removal of the vitelline membrane of sea urchin eggs. I. Use of dithiothreitol (Cleland Reagent). *Experimental Cell Research*, **61**(1), 64–68. doi: [10.1016/0014-4827\(70\)90257-0](https://doi.org/10.1016/0014-4827(70)90257-0)
- Ferrara, M. A., Di Caprio, G., Managó, S., De Angelis, A., Sirleto, L., Coppola, G. and De Luca, A. C. (2015a). Label-free imaging and biochemical characterization of bovine sperm cells. *Biosensors*, **5**(2), 141–157. doi: [10.3390/bios5020141](https://doi.org/10.3390/bios5020141)
- Ferrara, M. A., De Angelis, A., De Luca, A. C., Coppola, G., Dale, B. and Coppola, G. (2015b). Simultaneous holographic microscopy and Raman spectroscopy monitoring of human spermatozoa photodegradation. *IEEE Journal of Selected Topics in Quantum Electronics*, **22**(3), 27–34. doi: [10.1109/JSTQE.2015.2496265](https://doi.org/10.1109/JSTQE.2015.2496265)
- Gillot, I., Ciapa, B., Payan, P. and Sardet, C. (1991). The calcium content of cortical granules and the loss of calcium from sea urchin eggs at fertilization. *Developmental Biology*, **146**(2), 396–405. doi: [10.1016/0012-1606\(91\)90241-t](https://doi.org/10.1016/0012-1606(91)90241-t)
- Henson, J. H. and Begg, D. A. (1988). Filamentous actin organization in the unfertilized sea urchin egg cortex. *Developmental Biology*, **127**(2), 338–348. doi: [10.1016/0012-1606\(88\)90320-x](https://doi.org/10.1016/0012-1606(88)90320-x)
- Hyrskyluoto, A. and Vartiainen, M. K. (2020). Regulation of nuclear actin dynamics in development and disease. *Current Opinion in Cell Biology*, **64**, 18–24. doi: [10.1016/j.ceb.2020.01.012](https://doi.org/10.1016/j.ceb.2020.01.012)
- Johnson, J. D. and Epel, D. (1976). Intracellular pH and activation of sea urchin eggs after fertilisation. *Nature*, **262**(5570), 661–664. doi: [10.1038/262661a0](https://doi.org/10.1038/262661a0)
- Just, E. E. (1928). Initiation of development in Arbacia: IV. Some cortical reactions as criteria for optimum fertilization capacity and their significance for the physiology of development. *Protoplasma*, **5**(1), 97–126. doi: [10.1007/BF01604592](https://doi.org/10.1007/BF01604592)
- Just, E. E. (1939). *The biology of the cell surface*. P. Blakiston's Son & Co., Inc. PA.
- Kanatani, H. (1973). Maturation-inducing substance in starfishes. In *International Review of Cytology*, **35**, 253–298. doi: [10.1016/s0074-7696\(08\)60356-3](https://doi.org/10.1016/s0074-7696(08)60356-3)
- Kishimoto, T. (2018). MPF-based meiotic cell cycle control: Half a century of lessons from starfish oocytes. *Proceedings of the Japan Academy. Series B, Physical and Biological Sciences*, **94**(4), 180–203. doi: [10.2183/pjab.94.013](https://doi.org/10.2183/pjab.94.013)
- Lange, K. (1999). Microvillar  $\text{Ca}^{++}$  signaling: A new view of an old problem. *Journal of Cellular Physiology*, **180**(1), 19–34. doi: [10.1002/\(SICI\)1097-4652\(199907\)180:1<19::AID-JCP3>3.0.CO;2-K](https://doi.org/10.1002/(SICI)1097-4652(199907)180:1<19::AID-JCP3>3.0.CO;2-K)
- Lee, K., Wang, C., Spate, L., Murphy, C. N., Prather, R. S. and Machaty, Z. (2014). Gynogenetic activation of porcine oocytes. *Cell Rejuvenation*, **16**(2), 121–129. doi: [10.1089/cell.2013.0074](https://doi.org/10.1089/cell.2013.0074)
- Li, R. and Albertini, D. F. (2013). The road to maturation: Somatic cell interaction and self-organization of the mammalian oocyte. *Nature Reviews. Molecular Cell Biology*, **14**(3), 141–152. doi: [10.1038/nrm3531](https://doi.org/10.1038/nrm3531)
- Lim, D., Lange, K. and Santella, L. (2002). Activation of oocytes by latrunculin A. *FASEB Journal*, **16**(9), 1050–1056. doi: [10.1096/fj.02-0021com](https://doi.org/10.1096/fj.02-0021com)
- Limatola, N., Vasilev, F., Chun, J. T. and Santella, L. (2019). Sodium-mediated fast electrical depolarization does not prevent polyspermic fertilization in *Paracentrotus lividus* eggs. *Zygote*, **27**(4), 241–249. doi: [10.1017/S0967199419000364](https://doi.org/10.1017/S0967199419000364)
- Limatola, N., Vasilev, F., Santella, L. and Chun, J. T. (2020a). Nicotine induces polyspermy in sea urchin eggs through a non-cholinergic pathway modulating actin dynamics. *Cells*, **9**(1). doi: [10.3390/cells9010063](https://doi.org/10.3390/cells9010063)
- Limatola, N., Chun, J. T. and Santella, L. (2020b). Effects of salinity and pH of seawater on the reproduction of the sea urchin *Paracentrotus lividus*. *Biological Bulletin*, **239**(1), 13–23. doi: [10.1086/710126](https://doi.org/10.1086/710126)
- Limatola, N., Chun, J. T., Cherraben, S., Schmitt, J. L., Lehn, J. M. and Santella, L. (2021a). Effects of dithiothreitol on fertilization and early development in sea urchin. *Cells*, **10**(12). doi: [10.3390/cells10123573](https://doi.org/10.3390/cells10123573)
- Limatola, N., Chun, J. T. and Santella, L. (2021b). Fertilization and development of *Arbacia lixula* eggs are affected by osmolality conditions. *Biosystems*, **206**, 104448. doi: [10.1016/j.biosystems.2021.104448](https://doi.org/10.1016/j.biosystems.2021.104448)

- Limatola, N., Chun, J. T. and Santella, L. (2022a). Species-specific gamete interaction during sea urchin fertilization: Roles of the egg jelly and vitelline layer. *Cells*, **11**(19). doi: [10.3390/cells11192984](https://doi.org/10.3390/cells11192984)
- Limatola, N., Chun, J. T. and Santella, L. (2022b). Regulation of the actin cytoskeleton-linked  $\text{Ca}^{2+}$  signaling by intracellular pH in fertilized eggs of sea urchin. *Cells*, **11**(9). doi: [10.3390/cells11091496](https://doi.org/10.3390/cells11091496)
- Limatola, N., Chun, J. T., Schneider, S. C., Schmitt, J. L., Lehn, J. M. and Santella, L. (2023). The effect of acidic and alkaline seawater on the F-actin-dependent  $\text{Ca}^{2+}$  signals following insemination of immature starfish oocytes and mature eggs. *Cells*, **12**(5). doi: [10.3390/cells12050740](https://doi.org/10.3390/cells12050740)
- Liu, K., Zhao, Q., Li, B. and Zhao, X. (2022). Raman spectroscopy: A novel technology for gastric cancer diagnosis. *Frontiers in Bioengineering and Biotechnology*, **10**, 856591. doi: [10.3389/fbioe.2022.856591](https://doi.org/10.3389/fbioe.2022.856591)
- Managó, S., Valente, C., Mirabelli, P., Circolo, D., Basile, F., Corda, D. and De Luca, A. C. (2016). A reliable Raman-spectroscopy-based approach for diagnosis, classification and follow-up of B-cell acute lymphoblastic leukemia. *Scientific Reports*, **6**, 24821. doi: [10.1038/srep24821](https://doi.org/10.1038/srep24821)
- Managó, S., Mirabelli, P., Napolitano, M., Zito, G. and De Luca, A. C. (2018). Raman detection and identification of normal and leukemic hematopoietic cells. *Journal of Biophotonics*, **11**(5), e201700265. doi: [10.1002/jbio.201700265](https://doi.org/10.1002/jbio.201700265)
- Mangini, M., Ferrara, M. A., Zito, G., Managó, S., Luini, A., De Luca, A. C. and Coppola, G. (2023). Cancer metabolic features allow discrimination of tumor from white blood cells by label-free multimodal optical imaging. *Frontiers in Bioengineering and Biotechnology*, **11**, 1057216. doi: [10.3389/fbioe.2023.1057216](https://doi.org/10.3389/fbioe.2023.1057216)
- Maro, B., Johnson, M. H., Pickering, S. J. and Flach, G. (1984). Changes in actin distribution during fertilization of the mouse egg. *Journal of Embryology and Experimental Morphology*, **81**, 211–237. doi: [10.1242/dev.81.1.211](https://doi.org/10.1242/dev.81.1.211)
- Mazia, D., Schatten, G. and Steinhardt, R. (1975). Turning on of activities in unfertilized sea urchin eggs: Correlation with changes of the surface. *Proceedings of the National Academy of Sciences of the United States of America*, **72**(11), 4469–4473. doi: [10.1073/pnas.72.11.4469](https://doi.org/10.1073/pnas.72.11.4469)
- Meijer, L. and Guerrier, P. (1984). Maturation and fertilization in starfish oocytes. *International Review of Cytology*, **86**, 129–196. doi: [10.1016/s0074-7696\(08\)60179-5](https://doi.org/10.1016/s0074-7696(08)60179-5)
- Movasaghi, Z., Rehman, S. and Rehman, I. U. (2007). Raman spectroscopy of biological tissues. *Applied Spectroscopy Reviews*, **42**(5), 493–541. doi: [10.1080/05704920701551530](https://doi.org/10.1080/05704920701551530)
- Nekvapil, F., Brezeştean, I., Tomšić, S., Müller, C., Chiş, V. and Cîntă Pinzaru, S. (2019). Microsphere packages of carotenoids: Intact sea urchin eggs tracked by Raman spectroscopy tools. *Photochemical and Photobiological Sciences*, **18**(8), 1933–1944. doi: [10.1039/c9pp00181f](https://doi.org/10.1039/c9pp00181f)
- Nusco, G. A., Chun, J. T., Ercolano, E., Lim, D., Gragnaniello, G., Kyoizuka, K. and Santella, L. (2006). Modulation of calcium signalling by the actin-binding protein cofilin. *Biochemical and Biophysical Research Communications*, **348**(1), 109–114. doi: [10.1016/j.bbrc.2006.07.023](https://doi.org/10.1016/j.bbrc.2006.07.023)
- Pal, D., Ellis, A., Sepúlveda-Ramírez, S. P., Salgado, T., Terrazas, I., Reyes, G., De La Rosa, R., Henson, J. H. and Shuster, C. B. (2020). Rac and Arp2/3-nucleated actin networks antagonize rho during mitotic and meiotic cleavages. *Frontiers in Cell and Developmental Biology*, **8**(8), 591141. doi: [10.3389/fcell.2020.591141](https://doi.org/10.3389/fcell.2020.591141)
- Parrington, J., Davis, L. C., Galione, A. and Wessel, G. (2007). Flipping the switch: How a sperm activates the egg at fertilization. *Developmental Dynamics*, **236**(8), 2027–2038. doi: [10.1002/dvdy.21255](https://doi.org/10.1002/dvdy.21255)
- Perevedentseva, E., Krivokharchenko, A., Karmenyan, A. V., Chang, H. H. and Cheng, C. L. (2019). Raman spectroscopy on live mouse early embryo while it continues to develop into blastocyst *in vitro*. *Scientific Reports*, **9**(1), 6636. doi: [10.1038/s41598-019-42958-5](https://doi.org/10.1038/s41598-019-42958-5)
- Pollard, T. D. and Cooper, J. A. (2009). Actin, a central player in cell shape and movement. *Science*, **326**(5957), 1208–1212. doi: [10.1126/science.1175862](https://doi.org/10.1126/science.1175862)
- Puppo, A., Chun, J. T., Gragnaniello, G., Garante, E. and Santella, L. (2008). Alteration of the cortical actin cytoskeleton deregulates  $\text{Ca}^{2+}$  signaling, monospermic fertilization, and sperm entry. *PLOS ONE*, **3**(10), e3588. doi: [10.1371/journal.pone.0003588](https://doi.org/10.1371/journal.pone.0003588)
- Ramos, I. and Wessel, G. M. (2013). Calcium pathway machinery at fertilization in echinoderms. *Cell Calcium*, **53**(1), 16–23. doi: [10.1016/j.ceca.2012.11.011](https://doi.org/10.1016/j.ceca.2012.11.011)
- Rausch, V. and Hansen, C. G. (2020). The hippo pathway, YAP/TAZ, and the plasma membrane. *Trends in Cell Biology*, **30**(1), 32–48. doi: [10.1016/j.tcb.2019.10.005](https://doi.org/10.1016/j.tcb.2019.10.005)
- Roessl, U., Leitgeb, S., Pieters, S., De Beer, T. and Nidetzky, B. (2014). *In situ* protein secondary structure determination in ice: Raman spectroscopy-based process analytical tool for frozen storage of biopharmaceuticals. *Journal of Pharmaceutical Sciences*, **103**(8), 2287–2295. doi: [10.1002/jps.24072](https://doi.org/10.1002/jps.24072)
- Santella, L. and Chun, J. T. (2022). Structural actin dynamics during oocyte maturation and fertilization. *Biochemical and Biophysical Research Communications*, **633**, 13–16. doi: [10.1016/j.bbrc.2022.09.001](https://doi.org/10.1016/j.bbrc.2022.09.001)
- Santella, L., Vasilev, F. and Chun, J. T. (2012). Fertilization in echinoderms. *Biochemical and Biophysical Research Communications*, **425**(3), 588–594. doi: [10.1016/j.bbrc.2012.07.159](https://doi.org/10.1016/j.bbrc.2012.07.159)
- Santella, L., Limatola, N. and Chun, J. T. (2015). Calcium and actin in the saga of awakening oocytes. *Biochemical and Biophysical Research Communications*, **460**(1), 104–113. doi: [10.1016/j.bbrc.2015.03.028](https://doi.org/10.1016/j.bbrc.2015.03.028)
- Santella, L., Limatola, N. and Chun, J. T. (2020). Cellular and molecular aspects of oocyte maturation and fertilization: A perspective from the actin cytoskeleton. *Zoological Letters*, **6**(1), 5. doi: [10.1186/s40851-020-00157-5](https://doi.org/10.1186/s40851-020-00157-5)
- Sardet, C. (1984). The ultrastructure of the sea urchin egg cortex isolated before and after fertilization. *Developmental Biology*, **105**(1), 196–210. doi: [10.1016/0012-1606\(84\)90275-6](https://doi.org/10.1016/0012-1606(84)90275-6)
- Schatten, G. and Mazia, D. (1976). The penetration of the spermatozoon through the sea urchin egg surface at fertilization. Observations from the outside on whole eggs and from the inside on isolated surfaces. *Experimental Cell Research*, **98**(2), 325–337. doi: [10.1016/0014-4827\(76\)90444-4](https://doi.org/10.1016/0014-4827(76)90444-4)
- Short, K. W., Carpenter, S., Freyer, J. P. and Mourant, J. R. (2005). Raman spectroscopy detects biochemical changes due to proliferation in mammalian cell cultures. *Biophysical Journal*, **88**(6), 4274–4288. doi: [10.1529/biophysj.103.038604](https://doi.org/10.1529/biophysj.103.038604)
- Spudich, A., Wrenn, J. T. and Wessells, N. K. (1988). Unfertilized sea urchin eggs contain a discrete cortical shell of actin that is subdivided into two organizational states. *Cell Motility and the Cytoskeleton*, **9**(1), 85–96. doi: [10.1002/cm.970090109](https://doi.org/10.1002/cm.970090109)
- Steinhardt, R. A., Lundin, L. and Mazia, D. (1971). Bioelectric responses of the echinoderm egg to fertilization. *Proceedings of the National Academy of Sciences of the United States of America*, **68**(10), 2426–2430. doi: [10.1073/pnas.68.10.2426](https://doi.org/10.1073/pnas.68.10.2426)
- Terada, Y., Morito, Y., Tachibana, M., Morita, J., Nakamura, S. I., Murakami, T., Yaegashi, N. and Okamura, K. (2005). Cytoskeletal dynamics during mammalian gametogenesis and fertilization: Implications for human reproduction. *Reproductive Medicine and Biology*, **4**(3), 179–187. doi: [10.1111/j.1447-0578.2005.00103.x](https://doi.org/10.1111/j.1447-0578.2005.00103.x)
- Terasaki, M. (1996). Actin filament translocations in sea urchin eggs. *Cell Motility and the Cytoskeleton*, **34**, 48–56. doi: [10.1002/\(SICI\)1097-0169\(1996\)34:1<48::AID-CM5>3.0.CO;2-E](https://doi.org/10.1002/(SICI)1097-0169(1996)34:1<48::AID-CM5>3.0.CO;2-E)
- Tilney, L. G. and Jaffe, L. A. (1980). Actin, microvilli, and the fertilization cone of sea urchin eggs. *Journal of Cell Biology*, **87**(3 Pt. 1), 771–782. doi: [10.1083/jcb.87.3.771](https://doi.org/10.1083/jcb.87.3.771)
- Trimmer, J. S. and Vacquier, V. D. (1986). Activation of sea urchin gametes. *Annual Review of Cell Biology*, **2**, 1–26. doi: [10.1146/annurev.cb.02.110186.000245](https://doi.org/10.1146/annurev.cb.02.110186.000245)
- Vacquier, V. D. (2011). Laboratory on sea urchin fertilization. *Molecular Reproduction and Development*, **78**(8), 553–564. doi: [10.1002/mrd.21360](https://doi.org/10.1002/mrd.21360)
- Vasilev, F., Limatola, N., Park, D. R., Kim, U. H., Santella, L. and Chun, J. T. (2018). Disassembly of subplasmalemmal actin filaments induces cytosolic  $\text{Ca}^{2+}$  increases in *Astropecten aranciatus* eggs. *Cellular Physiology and Biochemistry*, **48**(5), 2011–2034. doi: [10.1159/000492523](https://doi.org/10.1159/000492523)
- Vasilev, F., Limatola, N., Chun, J. T. and Santella, L. (2019). Contributions of subolemmal acidic vesicles and microvilli to the intracellular  $\text{Ca}^{2+}$  increase

- in the sea urchin eggs at fertilization. *International Journal of Biological Sciences*, **15**(4), 757–775. doi: [10.7150/ijbs.28461](https://doi.org/10.7150/ijbs.28461)
- Vasilev, F., Ezhova, Y. and Chun, J. T. (2021). Signaling enzymes and ion channels being modulated by the actin cytoskeleton at the plasma membrane. *International Journal of Molecular Sciences*, **22**(19). doi: [10.3390/ijms221910366](https://doi.org/10.3390/ijms221910366)
- Wessel, G. M., Brooks, J. M., Green, E., Haley, S., Voronina, E., Wong, J., Zaydfudim, V. and Conner, S. (2001). The biology of cortical granules. *International Review of Cytology*, **209**, 117–206. doi: [10.1016/s0074-7696\(01\)09012-x](https://doi.org/10.1016/s0074-7696(01)09012-x)
- Whitaker, M. (2006). Calcium at fertilization and in early development. *Physiological Reviews*, **86**(1), 25–88. doi: [10.1152/physrev.00023.2005](https://doi.org/10.1152/physrev.00023.2005)
- Yin, H. L. and Janmey, P. A. (2003). Phosphoinositide regulation of the actin cytoskeleton. *Annual Review of Physiology*, **65**, 761–789. doi: [10.1146/annurev.physiol.65.092101.142517](https://doi.org/10.1146/annurev.physiol.65.092101.142517)
- Yonemura, S. and Mabuchi, I. (1987). Wave of cortical actin polymerization in the sea urchin egg. *Cell Motility and the Cytoskeleton*, **7**(1), 46–53. doi: [10.1002/cm.970070107](https://doi.org/10.1002/cm.970070107)
- Zeng, H. H., Xu, Z. H. and Wang, K. (1997). FT-Raman studies on the transformation of G-actin to F-actin, the binding of cisplatin and transplatin to F-actin and the effects of the conformation of F-actin. *International Journal of Biological Macromolecules*, **20**(2), 107–113. doi: [10.1016/s0141-8130\(96\)01144-0](https://doi.org/10.1016/s0141-8130(96)01144-0)